

## Systemic administration of a viral nanoparticle neoadjuvant prevents lung metastasis development through emergency myelopoiesis

Léa Bourguignon, Roxann Héту-Arbour, Tania Charpentier, Marilène Bolduc, Denis Leclerc, Krista M. Heinonen & Alain Lamarre

To cite this article: Léa Bourguignon, Roxann Héту-Arbour, Tania Charpentier, Marilène Bolduc, Denis Leclerc, Krista M. Heinonen & Alain Lamarre (2024) Systemic administration of a viral nanoparticle neoadjuvant prevents lung metastasis development through emergency myelopoiesis, *Oncolmunology*, 13:1, 2429846, DOI: [10.1080/2162402X.2024.2429846](https://doi.org/10.1080/2162402X.2024.2429846)

To link to this article: <https://doi.org/10.1080/2162402X.2024.2429846>



© 2024 The Author(s). Published with license by Taylor & Francis Group, LLC.



[View supplementary material](#)



Published online: 17 Nov 2024.



[Submit your article to this journal](#)



Article views: 244



[View related articles](#)




[View Crossmark data](#)

ORIGINAL RESEARCH

OPEN ACCESS



# Systemic administration of a viral nanoparticle neoadjuvant prevents lung metastasis development through emergency myelopoiesis

Léa Bourguignon<sup>a</sup>, Roxann Héту-Arbour<sup>a</sup>, Tania Charpentier<sup>a</sup>, Marilène Bolduc<sup>b</sup>, Denis Leclerc<sup>b</sup>, Krista M. Heinonen<sup>a</sup>, and Alain Lamarre<sup>a</sup> 

<sup>a</sup>Centre Armand-Frappier Santé Biotechnologie, Institut national de la recherche scientifique, Laval, QC, Canada; <sup>b</sup>Department of Microbiology, Infectiology and Immunology, Infectious Disease Research Center, Laval University, Quebec City, QC, Canada

## ABSTRACT

Cancer presents a significant public health concern, particularly in the context of metastatic disease. Surgical removal of primary tumors, while essential, can inadvertently heighten the risk of metastasis. Thus, there is a critical need for innovative neoadjuvant therapies capable of curtailing metastatic progression before or immediately following tumor resection. Addressing this imperative, the papaya mosaic virus nanoparticle (PapMV) has demonstrated potent immunostimulatory capabilities against both viruses and tumors, effectively hindering their proliferation. Our study reveals that PapMV exerts a protective effect against lung metastasis when administered systemically prior to tumor implantation or during the early stages of metastasis in various mouse models of cancer. This anti-tumor effect is initiated by the recruitment of myeloid cells in the lungs. These cells adopt a pro-inflammatory profile, secreting cytokines such as IFN- $\alpha$ , thus fostering a tumor microenvironment inhospitable to tumor progression. Crucially, this protective mechanism hinges on the presence of macrophages before treatment. TLR7 and IFN-I signaling pathways also play pivotal roles in this process. Furthermore, our findings demonstrate that PapMV triggers the activation of the bone marrow emergency response, which accounts for the influx of myeloid cells into the lungs. This study unveils a novel aspect of PapMV's functionality. By bolstering the immune system, PapMV confers robust protection against metastasis at an early stage of disease progression. This discovery holds promise for therapeutic intervention, particularly as a preemptive measure prior to or just after surgical intervention.

## ARTICLE HISTORY

Received 31 May 2024  
Revised 8 November 2024  
Accepted 11 November 2024

## KEYWORDS


Cancer immunotherapy;  
emergency myelopoiesis;  
metastasis prevention;  
neoadjuvant therapy;  
virus-based nanoparticle


## Introduction

In recent years, cancer research has witnessed remarkable strides, particularly in the development of new immunotherapies.<sup>1</sup> Plant virus nanoparticles (PVLPs) have emerged as a promising class of adjuvants capable of enhancing antitumoral immunity.<sup>2</sup> PVLPs, exemplified by the papaya mosaic virus nanoparticle (PapMV), possess inherent safety features while exhibiting high immunogenicity.<sup>3</sup> Our previous research demonstrated that PapMV nanoparticles are efficiently internalized by antigen-presenting cells (APCs), subsequently presented via MHC-I,<sup>4,5</sup> and activate various immune cells, leading to the secretion of pro-inflammatory cytokines.<sup>6</sup> Additionally, PapMV stimulates the development of an enhanced humoral or cellular immune response.<sup>7,8</sup> Specifically, the single-stranded RNA (ssRNA) molecule contained within PapMV nanoparticles is recognized by TLR7, thereby activating the Myd88-IRF5/7 signaling pathway leading to the secretion of IFN- $\alpha$ , which enhances the quality of the immune response elicited by vaccination.<sup>7</sup> In vitro studies using human cells have shown that PapMV induces the activation and expansion of T-CD8+ cells, secretion of pro-inflammatory cytokines,<sup>9</sup> and enhanced NK cytolytic activity.<sup>10,11</sup> Importantly, our investigations revealed that

PapMV exhibits anti-tumor effects in a melanoma mouse model, slowing tumor growth by recruiting immune cells, particularly tumor antigen-specific T-CD8+ cells in the tumor microenvironment (TEM), and producing pro-inflammatory cytokines.<sup>12</sup> Moreover, combining PapMV with anti-PD1 or DC-vaccination significantly enhances efficacy.<sup>12</sup> Finally, a Phase I clinical trial assessed the safety of intramuscular PapMV injection, reporting “no observed adverse effects” with doses ranging between 30 and 240  $\mu$ g per injection.<sup>13</sup> This presents a major advantage over imidazoquinolines, another class of TLR7/8 agonists, which can only be administered topically due to toxicity associated with other methods of administration.<sup>14</sup>

Metastases, owing to their intrinsic heterogeneity are particularly resistant to current therapies.<sup>15</sup> Their development correlates with aggressiveness and is associated with high morbidity and mortality rates.<sup>16,17</sup> Certain cancers, such as melanoma, breast, or colorectal cancer, have a propensity to metastasize to the lungs.<sup>18</sup> Surgical removal is a standard treatment for primary solid tumors, although it can induce local and systemic inflammation, creating a conducive environment for the development of metastases. In the present study, we are deciphering the immunostimulatory properties of PapMV to

**CONTACT** Alain Lamarre  [alain.lamarre@inrs.ca](mailto:alain.lamarre@inrs.ca)  Centre Armand-Frappier Santé Biotechnologie, Institut national de la recherche scientifique, 531, boul. des Prairies, Laval, QC H7V 1B7, Canada

 Supplemental data for this article can be accessed online at <https://doi.org/10.1080/2162402X.2024.2429846>

© 2024 The Author(s). Published with license by Taylor & Francis Group, LLC.

This is an Open Access article distributed under the terms of the Creative Commons Attribution-NonCommercial License (<http://creativecommons.org/licenses/by-nc/4.0/>), which permits unrestricted non-commercial use, distribution, and reproduction in any medium, provided the original work is properly cited. The terms on which this article has been published allow the posting of the Accepted Manuscript in a repository by the author(s) or with their consent.

identify applications where PapMV could potentially confer protection against metastasis establishment.

## Methods

### Mice

Female C57BL/6 mice (6–12 weeks old) and female Balb/c mice (6–12 weeks old) were purchased from the Jackson Laboratory. Female Tlr7 knockout (KO) mice (6–12 weeks old) were purchased from the Jackson Laboratory and bred in our animal facility. Type I IFN KO mice (Ifnar KO) (6–12 weeks old) were kindly provided by U. Kalinke (Institute for Experimental Infection Research, Braunschweig, Germany), and bred in our animal facility.

### Cell culture

Cell lines 4T1 (triple-negative breast cancer, #CRL-2539) and CT26 (colon carcinoma, #CRL-2638) were purchased from the ATCC, and grown in Roswell Park Memorial Institute (RPMI)-1640 medium (Wisent) supplemented with 10% fetal bovine serum (Wisent), 1% (10 mm) HEPES (Wisent) and 1% (1 mm) sodium pyruvate (Wisent). Cells were passaged every 2–3 days, at around 70% confluency.

### PapMV nanoparticles

PapMV nanoparticles were produced as previously described.<sup>9</sup> In brief, the coat protein (CP) open reading frame of PapMV was cloned into the plasmid pQE80, where the transcription of the PapMV CP gene was under the control of the strong T5 promoter in the bacterial strain BD-792. The PapMV CP is fused at its C-terminus to a 6×His purification tag, which allows for protein purification using immobilized metal affinity chromatography (IMAC). Lipopolysaccharides are removed by passing the IMAC-eluted protein through a Sartobind cartridge. The final concentration of LPS in the purified PapMV CP is less than 0.1 EU/mg and is considered negligible. The purified PapMV CP is used for self-assembly on a single-stranded RNA (ssRNA) corresponding to the first 1,517 nucleotides of the native PapMV virus RNA molecule where all ATG start codons have been mutated to TAG stop codons. The purified PapMV CP, at 2 mg/mL, is mixed with the ssRNA in a ratio of 20:1 (µg/µg) and gently stirred for 60 minutes at room temperature to induce self-assembly and production of nanoparticles. The PapMV nanoparticles are then subjected to tangential flow filtration (TFF) using a 100 kDa membrane to remove unassembled CP subunits and bacterial contaminants. The conversion of PapMV CP into nanoparticles is approximately 90%. The PapMV nanoparticles are concentrated to 5 mg/mL, filtered through a 0.22 µm filter, and stored in 10 mm Tris-HCl pH 7.9 at 4°C. We have documented stability for more than 8 years under these conditions. Each lot of PapMV nanoparticles is analyzed by dynamic light scattering (DLS) to confirm the size, which is approximately 80–100 nm in length. We also observe the PapMV nanoparticles using electron microscopy after staining with uranyl acetate to confirm their flexuous rod shape. Finally, we perform SDS-PAGE to ensure

the integrity of the CP subunit size. In all experiments, nanoparticles were diluted in 10 mm TRIS before use, and a similar volume of 10 mm TRIS was used as control.

### Treatments with PapMV

#### Visualization of nodules

100 µl of either 1 mg/mL PapMV in 10 mm TRIS, or 10 mm TRIS, were injected IV, 6 h before or 2 days after intravenous injection of  $3 \times 10^5$  4T1 cells or CT26 cells. At 17- or 20-days post-injection for 4T1 and CT26 respectively, lungs were harvested, washed with 3 mL PBS and fixed in Fekete's solution. Nodules were counted by visual assessment, and lungs were photographed. Note that dark spots on photographs indicate traces of blood and not necessarily metastatic nodules.

#### Immunomodulatory analysis

100 µl of either 1 mg/mL PapMV in 10 mm TRIS, or 10 mm TRIS, were injected IV. Blood, spleen, lungs and bone marrow were collected for immune analysis at 6 h, 24 h, 7 days and/or 14 days post-injection.

#### IFNAR blockade

$3 \times 10^5$  4T1 cells were injected IV. Twenty-four hours later, 500 µg of anti-mouse IFNAR1 antibody (BioXcell), or IgG1 control, were injected intraperitoneally (IP). Twenty-four hours later, 100 µl of either 1 mg/mL PapMV in 10 mm TRIS, or 10 mm TRIS, were injected IV. Twenty-four hours or 14 days later, blood, spleen, lungs and bone marrow were harvested for immune analysis, or nodule enumeration.

#### Macrophage depletion

$3 \times 10^5$  4T1 cells were injected IV. Twenty-four hours later, 200 µL of control or clodronate containing liposomes (Liposoma) were injected IP. After 24 h, 100 µl of either 1 mg/mL PapMV in 10 mm TRIS, or 10 mm TRIS, were injected IV. About 6 h, 24 h or 14 days later, blood, spleen and lungs were harvested for immune analysis or nodule enumeration.

#### Flow cytometry

Lungs, kidneys and liver were harvested, cut, digested and cells isolated according to the tumor dissociation kit protocol (Miltenyi, #130-096-730) and following gentleMACS™ Dissociator (Miltenyi) instructions. Cells were passed through a 70 µm cell strainer (Corning) as recommended by the manufacturer. Spleen was harvested, and crushed on a 100 µm cell strainer. Blood was collected in tubes containing PBS with 1 mm EDTA for labeling. Cell viability was assessed with Zombie Aqua (BioLegend). FC receptors blocking was achieved using an anti-CD16/32 antibody (BioXCell). Antibodies against surface antigens are listed in supplementary Table S1. For internal antigens, cells were first fixed with CytoPerm/CytoFix (BD Biosciences), then permeabilized with 1X PermWash (BD Biosciences), before labeling with antibodies (Supplementary Table 1). Bone marrow, spleen and blood cells were prepared as previously described.<sup>19,20</sup> The gating strategies for myeloid cells from lung and blood are illustrated in Supplementary Figure S1 and S2, respectively.<sup>33,34</sup> The

gating strategy for lymphoid cells in spleen, lung and blood is illustrated in Supplementary Figure S3. Hematopoietic stem and progenitor cells (HSPC) populations were determined as shown in Supplementary Figure S4, and antibodies used are listed in Supplementary Table S2. Data were acquired using a BDLSR Fortessa Flow Cytometer (BD Biosciences) and analyzed using FlowJo software (BD Biosciences).

### Colony assays

BM single-cell suspensions were prepared in IMDM supplemented with 10% FBS Premium (Wisent). Cells were seeded in 35 mm nonadherent petri dishes in methylcellulose-based medium M3434 ( $10^4$  cells/dish) (StemCell Technologies). Colonies were counted and identified based of their morphology after 10 days under an inverted microscope. Colonies were also collected and analyzed by flow cytometry.

### ELISA

Blood was placed in serum-separating tubes (Sarstedt) and centrifuged for 15 minutes at 10,000 rpm. Serum was collected and stored at  $-80^{\circ}\text{C}$ . Interferon- $\alpha$  assay was performed using the MAX™ Deluxe Set Mouse IFN- $\alpha$ 1 ELISA kit (BioLegend) according to the manufacturer's instructions. Cytokines and chemokines quantification was conducted using the proinflammatory focused 10-plex or 32-plex detection assays (Eve technologies).

### Statistics

Data were analyzed by comparing PapMV to the TRIS control, for each condition individually, with a Student's t test. Comparisons were statistically significant when  $p < 0.05$ .

## Results

### Systemic PapMV administration reduces metastasis implantation in the lungs

To investigate the impact of PapMV treatment on metastasis development, we used a model in which cancer cells are injected intravenously (IV) to mimic metastatic implantation in the lungs. We used the 4T1 mammary carcinoma and the CT26 colon carcinoma. These models are widely used surrogates for highly metastatic malignancies observed in humans, for which treatment options are currently limited.<sup>21,22</sup> PapMV, or TRIS were injected IV either 6 hours before or 2 days after IV injection of tumor cells in Balb/c mice. Mice were euthanized 17 days post-injection for 4T1 and 20 days post-injection for CT26 (Figure 1a), and their lungs were harvested and fixed to enumerate metastatic nodules. Lungs treated with PapMV showed significantly fewer metastases for both 4T1 (Figure 1b,c) and CT26 tumors (Figure 1d,e) compared to those treated with TRIS.

### Systemic PapMV administration induces pro-inflammatory myeloid cell recruitment to the lungs

To begin investigating the mechanisms underlying PapMV's ability to restrict metastasis implantation in the lungs, we analyzed immune cells from lung tissue, using flow cytometry after systemic PapMV administration. Compared to TRIS, PapMV led to a rapid and substantial increase in the proportions of myeloid cells within total CD45+ immune cells in the lungs 6 hours and 24 hours post-injection (Figure 2a,b). The proportions of total monocytes (Figure 2c,d) and particularly inflammatory monocytes significantly increased in the lungs following PapMV administration (Figure 2e,f), while proportions of resident monocytes decreased inversely (Figure 2e,g). Macrophage proportions remained unchanged 6 hours after PapMV injection but increased at 24 hours (Figure 2h,i), whereas neutrophils exhibited a rapid increase in proportions at 6 hours but returned to control levels at 24 hours (Figure 2j,k). To determine whether the increased proportions observed in the lungs resulted from cell infiltration, we calculated the absolute cell numbers of all analyzed populations. Variations in total myeloid cell numbers generally reflected changes in their relative proportions (Supplementary Figure S5a-f). To assess whether systemic PapMV administration promoted immune cell infiltration into the lungs from the peripheral circulation, we analyzed immune cell compositions in the blood 6 hours and 24 hours after PapMV injection. Consistent with lung observations, PapMV administration resulted in increased proportions of myeloid cells and inflammatory monocytes in the blood (Figure 2l-o), while proportions of Ly6C low monocytes remained unchanged at 6 hours and were reduced at 24 hours (Figure 2P). Proportions of blood neutrophils drastically increased 6 hours following treatment and returned to control levels at 24 hours (Figure 2q,r). These findings suggest that systemic PapMV administration leads to the rapid recruitment and infiltration of inflammatory myeloid cells into the lungs from the peripheral circulation. To investigate whether other peripheral organs exhibit a similar pattern of immune cell composition in response to PapMV administration, we analyzed myeloid cell populations in the kidneys and liver by flow cytometry. Interestingly, kidneys showed a similar profile as lungs with the rapid increase in the proportions of total myeloid cells (Figure S6a-b), total monocytes (Figure S6c-d), inflammatory monocytes (Figure S6e-f) and macrophages (Figure S6h) and a concomitant decrease in resident monocyte proportions (Figure S6e, g). In contrast, the liver showed an opposite response to PapMV administration with a reduction in total myeloid cells (Figure S6i-j), total monocytes (Figure S6k-l), inflammatory monocytes (Figure S6m-n) and macrophages (Figure S6p) and a concomitant increase in resident monocyte proportions (Figure S6m, o) 6 h post injection. We hypothesize that this opposite response of the liver may be due to its intrinsic tolerogenic nature<sup>23</sup>; however, further investigations, beyond the scope of this study, will be required to explore the mechanisms underlying this intriguing effect.

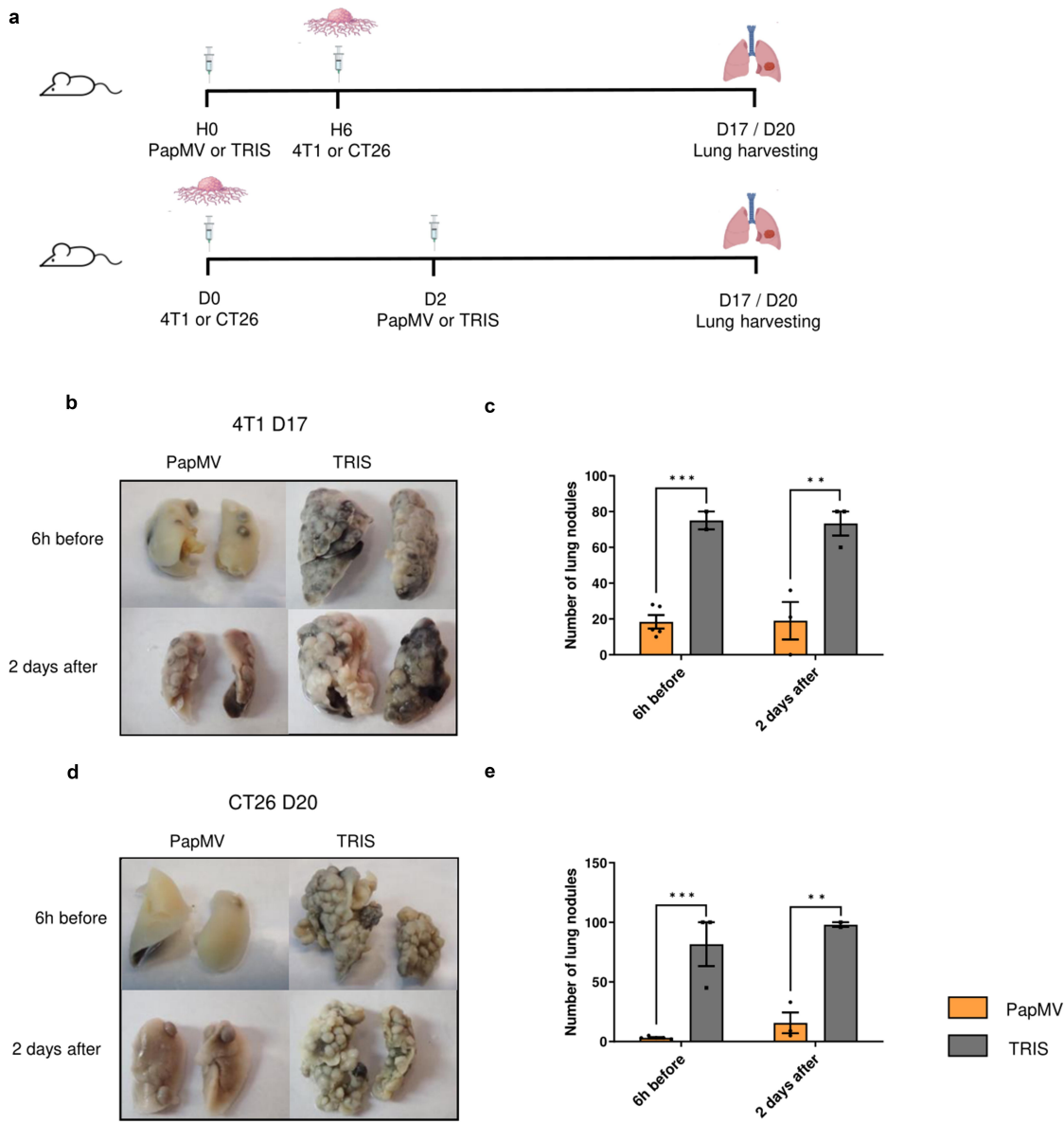


**Figure 1.** Systemic PapMV administration reduces metastasis implantation in the lungs. (a) Injection schedule for metastasis implantation model in Balb/c mice (created with BioRender.com). Balb/c mice were injected IV with PapMV or TRIS 6 h before (top) or 2 days after (bottom) IV inoculation with 4T1 or CT26 cells. (b) Lungs were harvested 17 days post injection of  $3 \times 10^5$  4T1 cells and (c) nodules were enumerated by visual inspection. (d) Lungs were harvested 20 days post injection of  $3 \times 10^5$  CT26 cells and (e) nodules enumerated as above. Values are means  $\pm$  SEM and compiled from two independent experiments ( $n = 6$  for 6h before,  $n = 3$  for 2 days after).

### Myeloid cell infiltration into the lungs depends on TLR7 and is partially dependent on IFN-I signaling

We showed previously that systemic administration of PapMV activates various immune cells in a TLR7-dependent manner leading to IFN- $\alpha$  production.<sup>7</sup> Thus, we next investigated whether TLR7 and IFN-I signaling also contributed to the recruitment of myeloid cells in the lungs. We administered PapMV or TRIS to *tlr7* knockout (KO) (TLR7) and *ifnar* KO (IFNAR) mice on the B6 genetic background. Proportions of myeloid cells (Figure 3a), total monocytes (Figure 3b), and specifically inflammatory monocytes (Figure 3c) increased in wildtype B6 mice following PapMV administration, similar to what

was observed in Balb/c mice (Figure 2). In contrast, the proportion of resident monocytes (Figure 3d) decreased, as also observed in the Balb/c model. Interestingly, these variations were abolished in TLR7 mice and only partially maintained in IFNAR mice. The same trend was observed with total macrophages (Figure 3e), while M2 macrophages decreased in the PapMV-treated group (Figure 3f,g). Moreover, PapMV treatment resulted in an increase in interstitial macrophages and a decrease in alveolar macrophages, which were not seen in TLR7 and IFNAR mice (Figure 3h-j). The increase in neutrophils induced by PapMV was also abolished in TLR7 mice (Figure 3k). In the blood, the proportions of myeloid cells (Figure 3l),

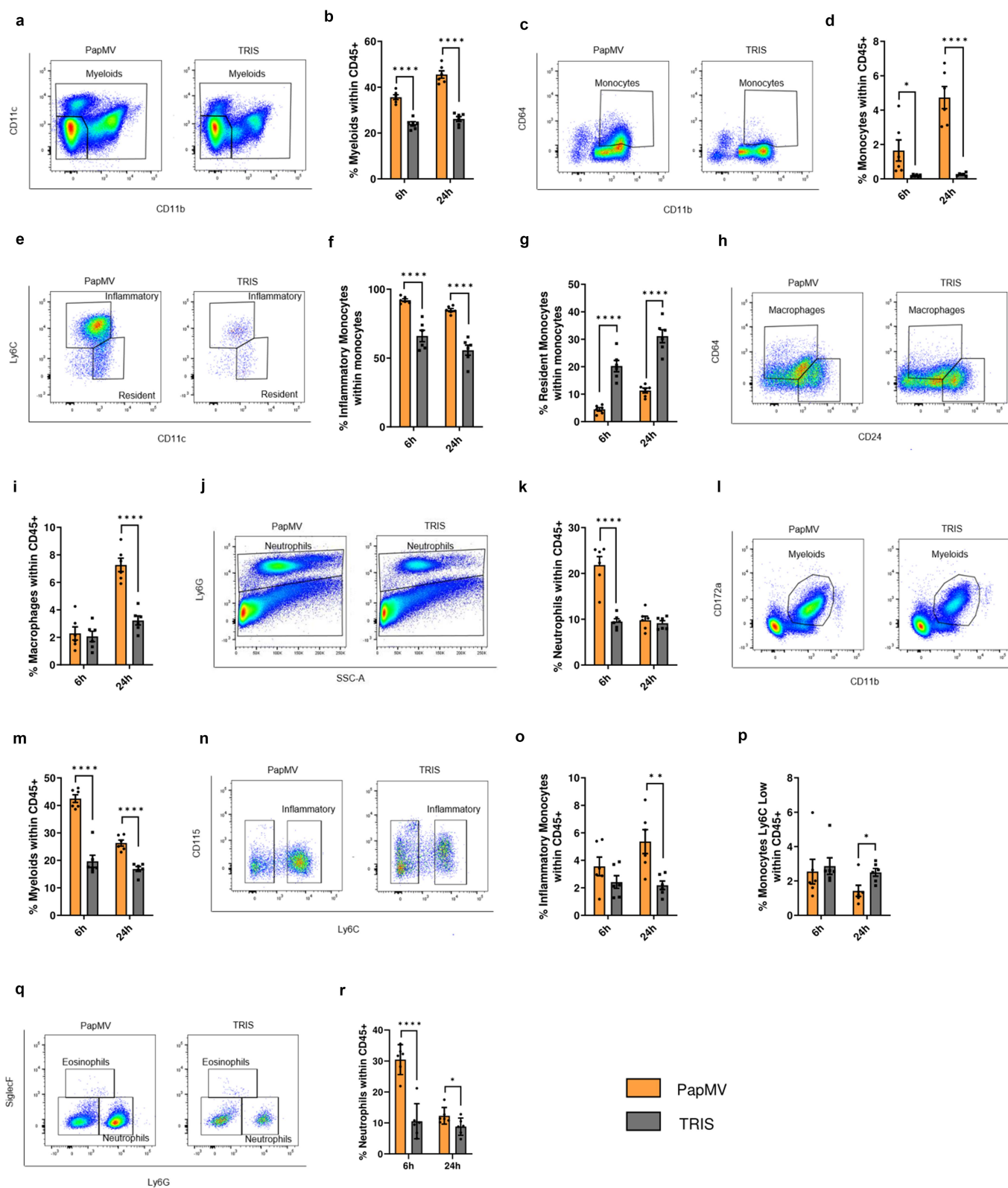


**Figure 2.** Systemic PapMV administration induces pro-inflammatory myeloid cell recruitment to the lungs. Balb/c mice were injected IV with PapMV or TRIS and euthanized 6h and 24h post-injection. (a-k) lungs and (l-r) blood were harvested for flow cytometric cell labeling. In lungs, proportions of (a-b) myeloid cells, (c-d) total monocytes, (e-f-g) monocyte subtypes, (h-i) macrophages, and (j-k) neutrophils were determined based on the cell population indicated on the Y axis. In blood, proportions of (l-m) myeloid cells, (n-o-p) monocyte subtypes, and (q-r) neutrophils were determined based on total CD45+ immune cells. A, C, E, H and N represent dot plots at 6h post-injection. J, L, and Q represent dot plots at 24h post-injection. Values are means  $\pm$  SEM and compiled from three independent experiments ( $n = 6$ ).

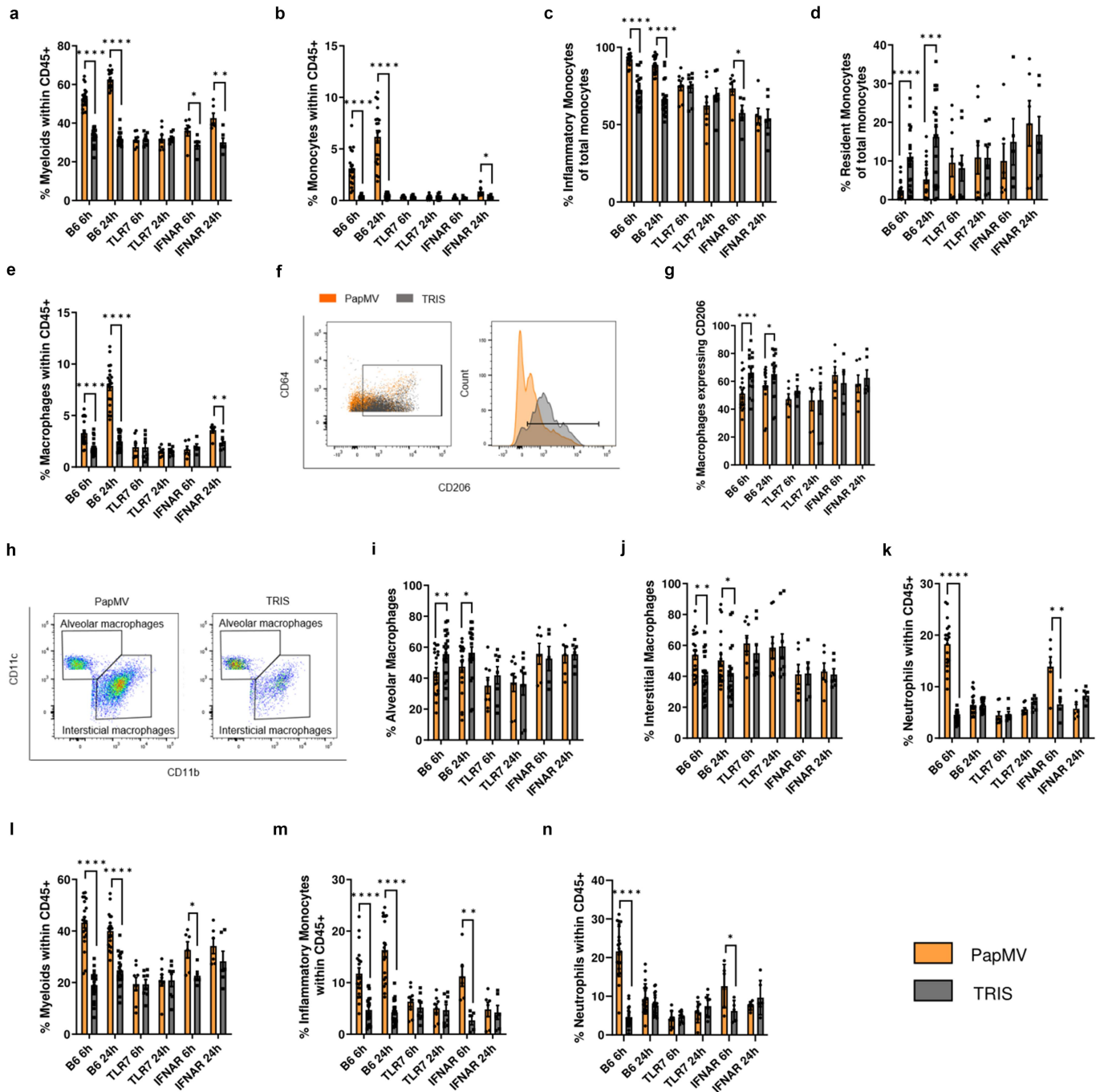


**Figure 3.** Myeloid cell infiltration into the lungs is dependent on TLR7 and partially dependent on IFN-I signaling. B6, TLR7, and IFNAR mice were injected IV with PapMV or TRIS and euthanized 6h and 24h post-injection. (a-k) lungs and (l-n) blood were harvested for flow cytometric cell labeling. In lungs, proportions of (a) myeloid cells, (b) total monocytes, (c-d) monocyte subtypes, (e) total macrophages, (f-g) M2 macrophages, (h-i) alveolar macrophages, (h-j) interstitial macrophages, and (k) neutrophils were determined based the cell population indicated on the Y axis. In blood, proportions of (l) myeloid cells, (m) inflammatory monocytes, and (n) neutrophils were determined based on total CD45+ immune cells. Values are means  $\pm$  SEM and compiled from three or four independent experiments ( $n = 20$  for B6,  $n = 8$  for TLR7, and  $n = 6$  for IFNAR).

inflammatory monocytes (Figure 3m), and neutrophils (Figure 3n) strongly increased with PapMV treatment, while in TLR7 mice, their proportions remained unchanged. IFNAR mice again showed an intermediate phenotype. Taken together, these results indicate that PapMV administration promotes the recruitment of pro-inflammatory myeloid cells to the lungs in a TLR7-dependent manner while mediators downstream of TLR7 engagement, other than IFN- $\alpha$ , also likely contribute to the

immunomodulatory effect of PapMV on the myeloid compartment.

### **Lymphoid cells are activated in the lungs of PapMV-treated mice in a TLR7- and ifnar-dependent manner**

We next examined the effect of systemic PapMV administration on lymphoid cell activation by assessing the upregulation

of CD69 and CD86 on NK cells, T-CD4 cells, T-CD8 cells, and B cells in the lungs. Although lymphoid cells were found in low numbers in the lungs of PapMV-treated mice (data not shown), those present exhibited high levels of activation (Supplementary Figure S7 a-k). Furthermore, lymphoid cell activation was strictly dependent on TLR7 and IFNAR.

### **Systemic PapMV injection induces pro-inflammatory cytokine production**

To determine whether immune cell activation and recruitment to the lungs are mediated by pro-inflammatory cytokines and chemokines, we measured serum concentrations of a large panel of cytokines and chemokines 6 and 24 hours following PapMV administration. PapMV injection resulted in the rapid secretion of several pro-inflammatory cytokines and chemokines in B6, IFNAR, and Balb/c mice, but not in TLR7 mice (Supplementary Figure S8 a-l).

### **Systemic PapMV injection activates bone marrow emergency response**

Hyperactive TLR7 signaling has been shown to lead to peripheral myeloid expansion due to an accumulation of myeloid precursor cells in the bone marrow (BM),<sup>24</sup> and ligands of other TLR, such as TLR4 ligand lipopolysaccharide, are well-established inducers of emergency myelopoiesis.<sup>25</sup> Thus, we evaluated the potential impact of PapMV injection on hematopoietic stem and progenitor cells (HSPC) in the bone marrow. Bone marrow HSPCs from PapMV-injected Balb/c mice upregulated the expression of the IFN-inducible Stem cell antigen-1 (Sca-1) at 24 h (Figure 4a,b). Although the numbers of CD48+ CD150- multipotent progenitor cells (MPP) and CD48- CD150+ hematopoietic stem cells were slightly decreased at the early time point (Figure 4c), they were rapidly restored to baseline levels (Figure 4d,e). Interestingly, in contrast to the decline in progenitor cell numbers as detected by flow cytometry, we observed an increase in their colony-forming ability at 24 h: bone marrow cells from PapMV-injected mice generated more monocytic and mast cell-like colonies (Figure 4f), and these colonies contained on average more cells, in particular, more CD11b+ CD11c+ monocyte-derived myeloid cells (Figure 4g), suggesting the activation of emergency myelopoiesis. We also evaluated the potential accumulation of HSPCs in the periphery and observed an increase in CD48+ CD150- MPPs, which include myeloid precursors, in the spleen of PapMV-injected mice (Figure 4h). Conversely, CD48+ CD150+ MPPs that give rise to erythroid and megakaryocytic lineages were slightly decreased (Figure 4h). Similar to the bone marrow, these changes in HSPC numbers at 24 h post-injection reverted to the baseline by day 7. The proportion of HSPCs in peripheral blood decreased after PapMV administration (Figure 4i), but we cannot determine if this was due to an increase in other cell types, such as myeloid cells (Figure 2) or the recruitment of HSPCs to the spleen and other organs. Of interest, there was also an increase in HSPC numbers in the lung at 24 h following PapMV administration (Figure 4j), suggesting that PapMV-induced myeloid differentiation

could also occur directly in the lung.<sup>26</sup> We next wanted to evaluate if the early PapMV-induced changes in HSPCs were also dependent on TLR7 and IFN-I. PapMV administration induced a decline in bone marrow MPPs and CD150+ stem cells in C57BL/6 (Figure 5a-c), similarly to Balb/c mice (Figure 4a,c) and it was abrogated in TLR7 KO mice but only partially in IFNAR KO mice. However, the peripheral response to PapMV was muted at 24 h in B6 as compared to Balb/c mice, and we observed no increase in CD48+ CD150- MPPs in the spleen (Figure 5d) or decline in peripheral blood HSPCs (Figure 5e). We hypothesize that this could be due to the differences in the kinetics of cytokine production between B6 and Balb/c mice (Supplementary Figure S7).

### **The immunomodulatory properties of PapMV are maintained when treatment is given two days after tumor implantation**

To investigate whether the immune-stimulating properties of PapMV are maintained in the presence of tumor cells in the lung microenvironment, Balb/c mice were injected IV with 4T1 cells followed two days later by systemic administration of PapMV or TRIS as described above. To determine the contribution of IFN-I in this experimental setup, a receptor-blocking (anti-IFNAR1) antibody was administered to some groups 24 hours before PapMV treatment. Mice were euthanized on day 3 or day 17 (Figure 6a). Mice treated with PapMV and receiving control immunoglobulin showed a drastic reduction in the number of lung metastases on day 17 compared to TRIS controls (Figure 6b,c). Strikingly, however, in mice receiving anti-IFNAR1 antibody, the anti-metastatic property of PapMV treatment was completely abolished. Importantly, the proportions of myeloid cells (Figure 6d) and monocytes (Figure 6e) in the lungs 24 hours following PapMV administration were significantly increased compared to controls, as was also observed in the lungs in the absence of tumor cells (Figure 2b,d). However, this effect was lost following IFNAR blockade. The increase in inflammatory monocytes (Figure 6f), as well as the decrease in resident monocytes (Figure 6g), denoted in the PapMV-treated group in the absence of tumor cells, were still evident in the tumor microenvironment, albeit in lower proportions. When IFN-I receptor is blocked, the effect is completely reversed. Additionally, the increase in macrophage proportions 24 hours after PapMV injection was conserved in this setting and was abrogated with anti-IFNAR treatment (Figure 6h). Similar results were observed in the blood (Figure 6i-j). Finally, PapMV treatment triggered the secretion of IFN- $\alpha$  (Figure 6k), TNF- $\alpha$  (Figure 6l), IL-6 (Figure 6m), and MCP-1 (Figure 6n), albeit in lower concentrations than those measured in tumor-free animals (Supplementary Figure S7a, d, e, and j, respectively) an effect that was abolished when IFN-I receptor was blocked. These results suggest that blocking IFNAR signaling is sufficient to entirely abolish the anti-metastatic effect of PapMV. More importantly, they demonstrate that PapMV's immunomodulatory properties are maintained when tumor cells are already implanted in the lung microenvironment.



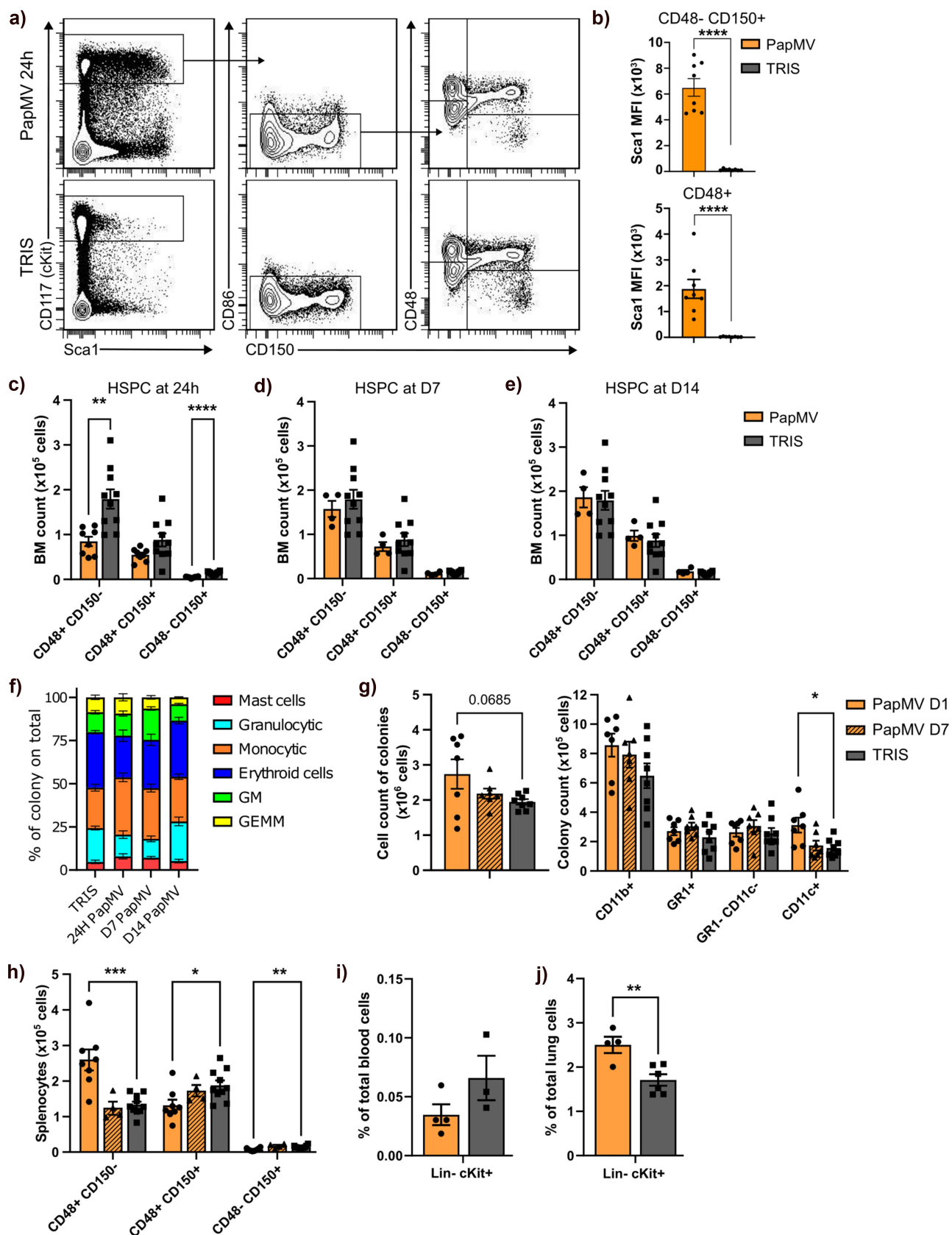


**Figure 4.** Systemic PapMV injection promotes the differentiation of hematopoietic stem cells into myeloid cells. Balb/c mice were injected IV with PapMV or TRIS and were euthanized 24h, day-7 or day-14 post-injection. (a-g) bone marrow, (j) spleen, (i) blood and (j) lung were analyzed for their HSPC composition. (a) Flow cytometry analysis of bone marrow progenitors. (b) Sca1 mean fluorescence intensity (MFI) on CD48+ and CD48- CD150+ cells at 24 hours post-injection. (c-e) number of CD48+ CD150-, CD48+ CD150+ and CD48- CD150+ cells in BM at (c) 24 hours, (d) 7 days and (e) 14 days post-injection. (f) Ratio of colony types over the total having grown from  $10^4$  BM cells 24h post-injection plated in M3434 methylcellulose-based medium (GM : granulocyte/macrophage colony; GEMM : granulocyte/erythroid/macrophage/megakaryocyte colony). (g) Flow cytometry analysis of colonies from 24 hours and 7 days post-injection of BM cells. Number of total cells from colony assay (left panel) and number of CD11b+ cells and granulocytes (GR1+ CD11c- cells), monocytes (GR1- CD11c- cells) and dc-like (GR1- CD11c+) sub-populations within

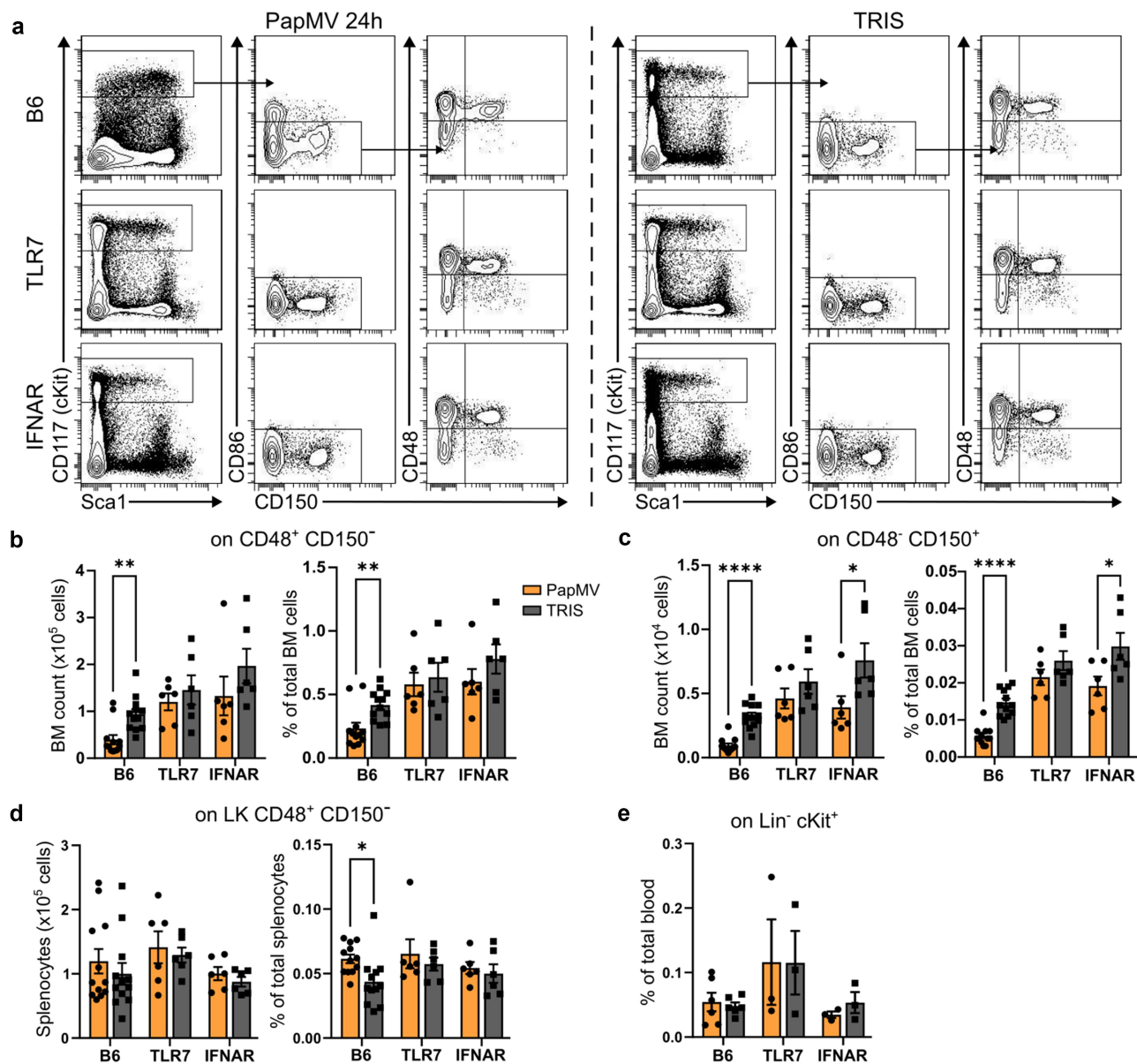


**Figure 5.** The production of new myeloid cells, in the bone marrow, is dependent on TLR7 and partially dependent on IFN-I signaling. (a) Flow cytometry analysis of bone marrow progenitors from representative B6, TLR7 KO and IFNAR KO mice at 24h post-PapMV-injection (left panels) and littermate mice injected with TRIS (right panels). Number (left panel) and percentage (right panel) of (b) CD48<sup>+</sup> CD150<sup>-</sup> and (c) CD48<sup>-</sup> CD150<sup>+</sup> cells in BM at 24 hours post-PapMV-injection. (d) Number (left panel) and percentage (right panel) of CD48<sup>+</sup> CD150<sup>-</sup> cells in splenocytes at 24 hours post-PapMV-injection. (e) Percentage of lin<sup>-</sup> cKit<sup>+</sup> blood cells at 24 hours post-PapMV-injection. Values are means  $\pm$  SEM and are compiled from three independent experiments. Blood results are from pooled mice (2 animals per data) to increase cell numbers. The B6 data are compiled from all the IFNAR KO and TLR7 KO experiments.

### Role of macrophages in the anti-metastatic properties of PapMV

To investigate the role of macrophages in initiating the remodeling of the immune landscape of the lung microenvironment in response to PapMV treatment, we analyzed the immune composition of lungs from PapMV-treated mice with or without macrophage depletion using clodronate-containing

liposomes (Figure 7a). While PapMV induced a rapid increase in total monocyte proportions in the lungs of animals receiving control liposomes, this increase was reduced in macrophage-depleted groups 6 hours following treatment whereas the reduction was less pronounced at 24 hours (Figure 7b). Inflammatory monocytes were slightly increased at 24 hours while resident monocytes inversely decreased following

the CD11b<sup>+</sup> cells (right panel). (h) Number of CD48<sup>+</sup> CD150<sup>-</sup>, CD48<sup>+</sup> CD150<sup>+</sup> and CD48<sup>-</sup> CD150<sup>+</sup> cells in splenocytes at 24 hours and 7 days post-injection. (i-j) percentage of lin<sup>-</sup> cKit<sup>+</sup> cells over total (i) blood cells and (j) lung cells at 24 hours post-injection. Values are means  $\pm$  SEM and are compiled from three independent experiments for 24 hours BM, splenocytes and blood data, and two independent experiments for colony assays (CFU and flow cytometry), and one experiment for 7 and 14 days BM data, 7 days splenocytes data and 24 hours lungs data. Blood results are from pooled mice (2 animals per n showed) to increase cell numbers. The control values are compiled from B6 data from 24 hours, 7 days and 14 days controls.

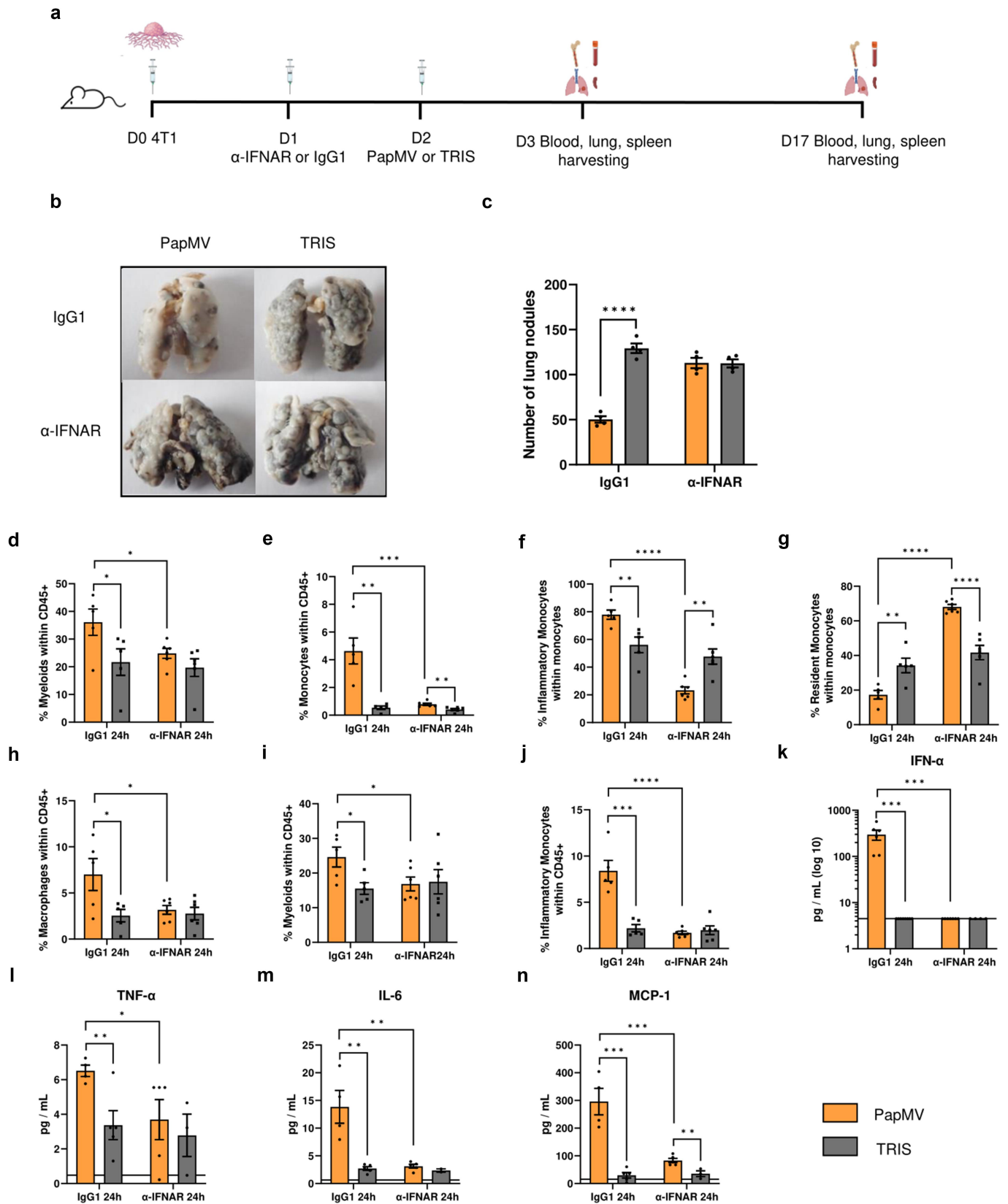


**Figure 6.** The immunomodulatory properties of PapMV are maintained when treatment is given two days after tumor implantation. (a) Injection schedule for metastasis implantation model in Balb/c mice (created with BioRender.com). Balb/c mice were injected IV with  $3 \times 10^5$  4T1 cells, 24 hours later they were treated with an  $\alpha$ -ifnar or IgG1 control antibody. 24 hours later they were injected IV with PapMV or TRIS. Mice were euthanized at D3 or D17. (b) Images and (c) numbers of lung metastases at D17 following treatment with PapMV or TRIS. At D3, (d-h) lungs and (i-j) blood were harvested for flow cytometric cell labeling. In the lungs, proportions of (d) myeloid cells, (e) total monocytes, (f) inflammatory monocytes, (g) resident monocytes, and (h) macrophages were determined based on the cell population indicated on the Y axis. In the blood, the proportion of (i) myeloid cells and (j) inflammatory monocytes were determined based on total CD45+ immune cells. Serum was collected 24h following PapMV treatment and (k) ifn- $\alpha$ , (l) tnf- $\alpha$ , (m) IL-6 and (n) MCP-1 concentrations were measured. Values are means  $\pm$  SEM and compiled from two independent experiments ( $n = 6$ ).

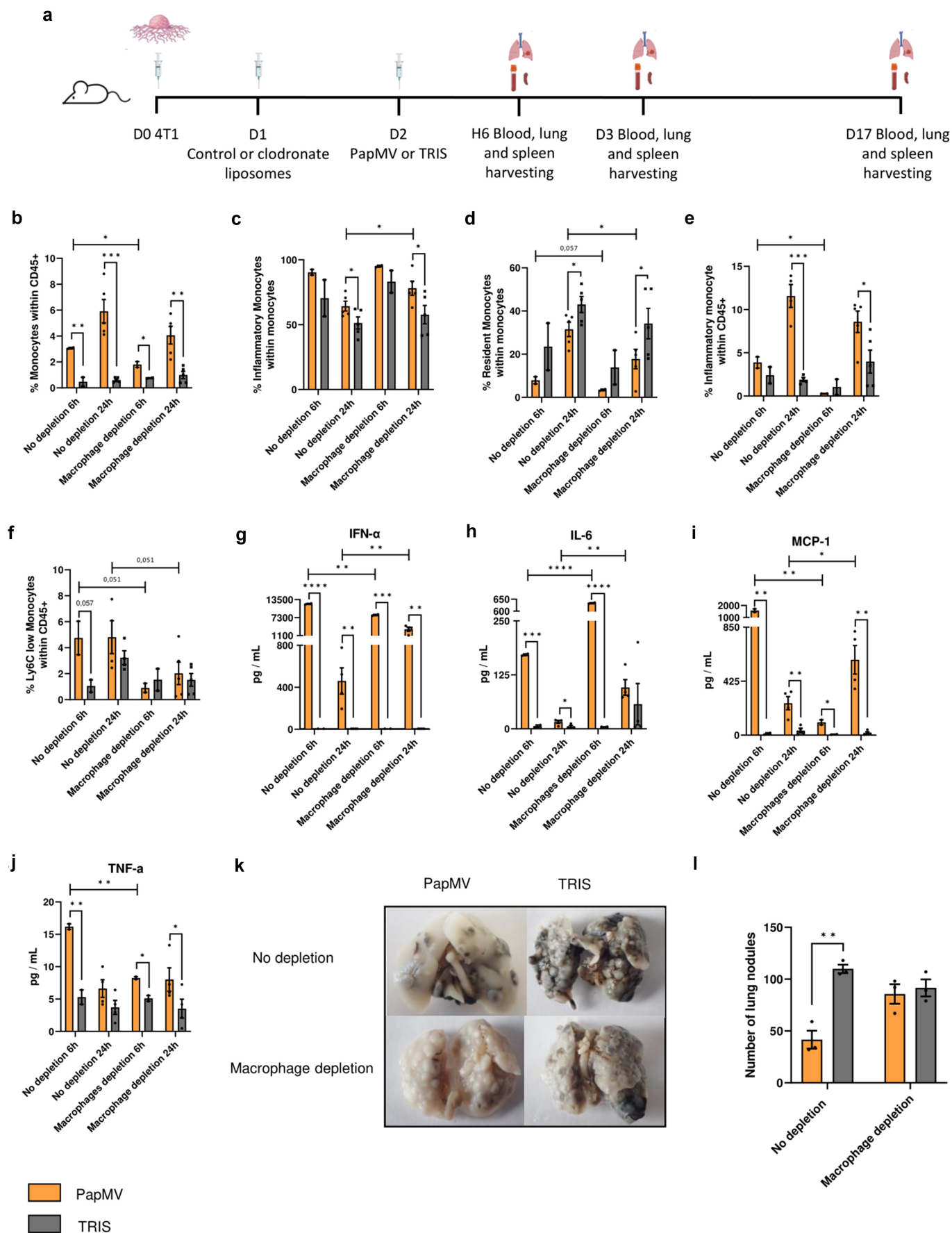


**Figure 7.** Role of macrophages in the anti-metastatic properties of PapMV. (a) Injection schedule for the metastasis implantation model in Balb/c mice (created with BioRender.com). Balb/c mice were injected IV with  $3 \times 10^5$  4T1 cells. After 24 hours, they received IP administration of control or clodronate containing liposomes. Subsequently, 24 hours later, they were injected IV with PapMV or TRIS. Mice were euthanized at 6 hours, 24 hours, or on day 17. At 6 hours and 24 hours (b-d) lungs and

macrophage depletion (Figure 7c,d, respectively). Depletion of macrophages reduced the proportion of inflammatory monocytes in the blood 6 hours and 24 hours after PapMV treatment (Figure 7e). Similar results were obtained for Ly6C low monocytes (Figure 7f). IFN- $\alpha$  production was significantly reduced following macrophage depletion 6 hours post-treatment indicative of a role for macrophages in sensing PapMV and early IFN- $\alpha$  secretion (Figure 7g).<sup>12</sup> Unexpectedly, IL-6 concentrations significantly increased in macrophage-depleted groups compared to controls, possibly due to a compensatory effect from other IL-6-producing cells (Figure 7h). Finally, MCP-1 and TNF- $\alpha$  serum concentrations were generally reduced in macrophage-depleted groups (Figure 7i,j). PapMV treatment led to a significant reduction in the number of metastatic nodules in the group receiving control liposomes (Figure 7k, l). Strikingly, however, when macrophages were depleted, this reduction was no longer observed. These results collectively indicate that macrophages play a crucial role in the anti-metastatic properties of PapMV by modulating the immune composition of lung infiltrates.

## Discussion

Metastasis poses a significant public health challenge due to the scarcity of effective therapies that impede its development or progression.<sup>27</sup> Virus-like particles used as immune adjuvants offer a promising avenue in cancer immunotherapy. Our findings reveal that PapMV significantly reduces lung metastasis development across tumor models and administration schedules, suggesting efficacy independent of cancer type. PapMV administration led to increased myeloid cell percentages in the lungs, particularly inflammatory monocytes, macrophages, and neutrophils, alongside elevated absolute numbers. TLR7 and IFN-I receptor absence abolish these effects, underlining their significance in myeloid recruitment and PapMV's overall impact. However, other danger/stress signals downstream of TLR7 signaling could also contribute to the immunomodulatory properties of PapMV. In mice receiving PapMV, the proportions of CD206 expressing M2 macrophages significantly decreased. Alveolar macrophages also decreased, while interstitial macrophages increased, potentially contributing to lung inflammation. Several therapies enabling M2-to-M1 polarization have been developed and show efficacy in colorectal cancer, including R848, a TLR7/8 agonist,<sup>28</sup> and in melanoma, resiquimod, another TLR7/8 agonist.<sup>29</sup> In the lungs, only DNA-damaging molecules such as hydroxychloroquine were shown to induce M1 polarization.<sup>30</sup> PapMV appears to efficiently skew monocyte differentiation and macrophage polarization toward a pro-inflammatory profile that hinders metastasis development. Moreover, PapMV treatment induced

the production of several cytokines and chemokines, associated with pro-inflammatory responses. Chronic production of these cytokines is associated with a poor prognosis in many cancers, enabling invasion and metastasis.<sup>31</sup> In our study, however, PapMV generates only a transient response, which diminishes as early as 24 hours after injection. Therefore, PapMV promotes acute inflammation and stimulates immune activation protecting against metastasis development without the deleterious risk associated with chronic exposure to inflammatory mediators. Previous studies have demonstrated that TLR7 signaling can lead to peripheral myeloid expansion, primarily through the accumulation of myeloid precursor cells in the bone marrow.<sup>24</sup> TLR7 activation leads to emergency myelopoiesis, with immunostimulation in the lungs.<sup>32</sup> PapMV-injected mice exhibited a transient decline in certain progenitor cell populations, followed by a rapid restoration to baseline levels. Intriguingly, despite this transient decline, there was a notable increase in the colony-forming ability of these cells, particularly toward monocytic and mast cell-like lineages, indicative of emergency monopoiesis activation. This phenomenon extended beyond the bone marrow, as evidenced by the accumulation of myeloid precursors in the spleen and, notably, in the lung, suggesting the potential for direct myeloid differentiation within the pulmonary tissue. To our knowledge, this is the first demonstration of a neoadjuvant therapy activating emergency myelopoiesis to prevent metastasis development.

Remarkably, PapMV conserved its immunomodulatory properties when administered 2 days after tumor implantation. This effect was completely abolished when the IFN-I receptor was blocked. These findings underscore the effectiveness of PapMV as a therapy against metastasis. Notably, previous studies compared PapMV to R837, a TLR7 agonist, in subcutaneous or metastatic melanoma cases, demonstrating PapMV's superior ability to induce immune responses against cancer cells.<sup>12</sup> Moreover, in human PBMCs, PapMV and the TLR7 agonist imiquimod elicited similar cell activation.<sup>11</sup> One of the key advantages of PapMV over small molecule TLR7 agonists lies in its selective capacity to stimulate a focused immune response as opposed to the systemic activation seen with classical TLR7 agonists which is associated with their cytotoxicity profile.<sup>14</sup>

Our investigation provides valuable insights into the role of macrophages in orchestrating the immune response to PapMV treatment and its subsequent impact on metastasis inhibition. PapMV prompts a swift increase in total monocyte proportions in the lungs, a response that was attenuated in macrophage-depleted groups, indicating the pivotal involvement of macrophages in this process. Additionally, macrophage depletion led to reduced proportions of inflammatory monocytes in the blood and a reduction in the concentration of several cytokines, underscoring the pivotal role of macrophages in sensing PapMV and facilitating early cytokine secretion. These

(e, f) blood were harvested for flow cytometric cell labeling. In the lungs, proportions of (b) monocytes and (c-d) monocyte subtypes were determined based the cell population indicated on the Y axis. In the blood, proportions of (e) inflammatory monocytes and (f) Ly6C low monocytes were determined based on total CD45+ immune cells. Serum was collected 6 hours and 24 hours following PapMV treatment and (g) ifn- $\alpha$ , (h) IL-6, (i) MCP-1, and (j) tnf- $\alpha$  concentrations were measured. (k) Lung metastases were visualized at D17 and (l) enumerated. Values are means  $\pm$  SEM and compiled from two independent experiments. ( $n = 2$  for 6h,  $n = 4$  for 24h).

findings underscore the intricate interplay between macrophages, immune modulation, and metastasis inhibition induced by PapMV, paving the way for further elucidation of the complex mechanisms underlying its therapeutic efficacy. Although not directly investigated in this study, we hypothesize that T cells, which are highly activated in the lungs of PapMV-treated mice, contribute to the anti-metastatic effect observed following PapMV administration.

In summary, our findings underline PapMV's potential as an effective therapy against metastasis. This therapeutic approach holds promise as a strategy to mitigate metastasis occurrence across various malignancies following tumor resection surgery and warrants further investigation and clinical translation to harness its full therapeutic potential.

## Acknowledgments

The authors wish to thank Jessy Tremblay (INRS) for his help with flow cytometry analyses.

## Disclosure statement

No potential conflict of interest was reported by the author(s).

## Funding

This work was supported by operating grants from the Canadian Institutes for Health Research (CIHR) to AL [MOP-89833], KMH [PJT-148614] and DL [298143 and 485777]. A. Lamarre holds the Jeanne and J.-Louis Lévesque research chair in immunovirology from the J.-Louis Lévesque Foundation.

## ORCID

Alain Lamarre  <http://orcid.org/0000-0002-7913-871X>

## Authors' contributions

LB, RH-A, TC and KMH conducted and performed experiments. MB and DL provided key reagents. AL and KMH supervised this study. LB, RH-A, KMH, and AL analyzed the data and wrote the manuscript.

## Availability of data and material

Data are available on reasonable request. The original dataset is available on request from the corresponding author.

## Consent for publication

All authors consent to present the information and data contained in this submission.

## Ethics approval

Animal experiments were conducted following the guidelines of the Canadian Council on Animal Care. All animal experiments were reviewed and approved by the Institutional Animal Care Committee of the Institut national de la recherche scientifique.

## Abbreviations

APC	Antigen-presenting cell
BM	Bone marrow
CTL	Cytotoxic T lymphocyte
GEMM	Granulocyte erythroid macrophage megakaryocyte colony
GM	Granulocyte macrophage colony
HSPC	Hematopoietic stem and progenitor cell
IP	Intraperitoneal injection
IV	Intravenous injection
MPP	Multipotent progenitor cell
PapMV	Papaya mosaic virus nanoparticle
PRR	Pattern recognition receptor
PVLP	Plant virus nanoparticle
Sca-1	Stem cell antigen-1
TAM	Tumor-associated macrophage
TLR	Toll-like receptor
TME	Tumor microenvironment

## References

- Lin D, Shen Y, Liang T. Oncolytic virotherapy: basic principles, recent advances and future directions. *Sig Transduct Target Ther*. 2023;8(1):156. doi:10.1038/s41392-023-01407-6.
- Shahgolzari M, Venkataraman S, Osano A, Akpa PA, Hefferon K. Plant virus nanoparticles combat cancer. *Vaccines (Basel)*. 2023;11(8):1278. doi:10.3390/vaccines11081278.
- Lebel ME, Chartrand K, Leclerc D, Lamarre A. Plant viruses as nanoparticle-based vaccines and adjuvants. *Vaccines (Basel)*. 2015;3(3):620–637. doi:10.3390/vaccines3030620.
- Lacasse P, Denis J, Lapointe R, Leclerc D, Lamarre A. Novel plant virus-based vaccine induces protective cytotoxic T-lymphocyte-mediated antiviral immunity through dendritic cell maturation. *J Virol*. 2008;82(2):785–794. doi:10.1128/JVI.01811-07.
- Hanafi LA, Bolduc M, Gagné MÈL, Dufour F, Langelier Y, Boulassel M-R, Routy J-P, Leclerc D, Lapointe R. Two distinct chimeric potexviruses share antigenic cross-presentation properties of MHC class I epitopes. *Vaccine*. 2010;28(34):5617–5626. doi:10.1016/j.vaccine.2010.06.024.
- Savard C, Guérin A, Drouin K, Bolduc M, Laliberté-Gagné M-E, Dumas M-C, Majeau N, Leclerc D. Improvement of the trivalent inactivated flu vaccine using PapMV nanoparticles. *PLoS One*. 2011;6(6):e21522. doi:10.1371/journal.pone.0021522.
- Lebel ME, Daudelin J-F, Chartrand K, Tarrab E, Kalinke U, Savard P, Labrecque N, Leclerc D, Lamarre A. Nanoparticle adjuvant sensing by TLR7 enhances CD8+ T cell-mediated protection from listeria monocytogenes infection. *J Immunol*. 2014;192(3):1071–1078. doi:10.4049/jimmunol.1302030.
- Denis J, Acosta-Ramirez E, Zhao Y, Hamelin M-E, Koukavica I, Baz M, Abed Y, Savard C, Pare C, Lopez Macias C, et al. Development of a universal influenza a vaccine based on the M2e peptide fused to the papaya mosaic virus (PapMV) vaccine platform. *Vaccine*. 2008;26(27–28):3395–3403. doi:10.1016/j.vaccine.2008.04.052.
- Mathieu C, Rioux G, Dumas M-C, Leclerc D. Induction of innate immunity in lungs with virus-like nanoparticles leads to protection against influenza and Streptococcus pneumoniae challenge. *Nanomedicine*. 2013;9(7):839–848. doi:10.1016/j.nano.2013.02.009.
- Leclerc D, Beauseigle D, Denis J, Morin H, Paré C, Lamarre A, Lapointe R. Proteasome-independent major histocompatibility complex class I cross-presentation mediated by papaya mosaic virus-like particles leads to expansion of specific human T cells. *J Virol*. 2007;81(3):1319–1326. doi:10.1128/JVI.01720-06.
- Carignan D, Herblot S, Laliberté-Gagné M-È, Bolduc M, Duval M, Savard P, Leclerc D. Activation of innate immunity in primary human cells using a plant virus derived nanoparticle TLR7/8 agonist. *Nanomedicine*. 2018;14(7):2317–2327. doi:10.1016/j.nano.2017.10.015.

12. Lebel ME, Chartrand K, Tarrab E, Savard P, Leclerc D, Lamarre A. Potentiating cancer immunotherapy using papaya mosaic virus-derived nanoparticles. *Nano Lett.* 2016;16(3):1826–1832. doi:10.1021/acs.nanolett.5b04877.
13. Langley J, Pastural E, Halperin S, McNeil S, ElSherif M, MacKinnon-Cameron D, Ye L, Grange C, Thibodeau V, Caillhier J-F, et al. A randomized controlled study to evaluate the safety and reactogenicity of a novel rVLP-based plant virus nanoparticle adjuvant combined with seasonal trivalent influenza vaccine following single immunization in healthy adults 18–50 years of age. *Vaccines (Basel).* 2020;8(3):393. doi:10.3390/vaccines8030393.
14. Engel AL, Holt GE, Lu H. The pharmacokinetics of toll-like receptor agonists and the impact on the immune system. *Expert Rev Clin Pharmacol.* 2011;4(2):275–289. doi:10.1586/ecp.11.5.
15. Steeg PS. Targeting metastasis. *Nat Rev Cancer.* 2016;16(4):201–218. doi:10.1038/nrc.2016.25.
16. Dillekås H, Rogers MS, Straume O. Are 90% of deaths from cancer caused by metastases? *Cancer Med.* 2019;8(12):5574–5576. doi:10.1002/cam4.2474.
17. Fidler IJ. The biology of cancer metastasis. *Semin Cancer Biol.* 2011;21(2):71. doi:10.1016/j.semcancer.2010.12.004.
18. Fidler IJ. The pathogenesis of cancer metastasis: the ‘seed and soil’ hypothesis revisited. *Nat Rev Cancer.* 2003;3(6):453–458. doi:10.1038/nrc1098.
19. Hetu-Arbour R, Bouali S, Heinonen KM. Experimental competitive bone marrow transplant assays. *Methods Mol Biol.* 2021;2185:195–214.
20. Kwarteng EO, Heinonen KM. Competitive transplants to evaluate hematopoietic stem cell fitness. *J Vis Exp.* 2016;(114). doi:10.3791/54345-v.
21. Schrörs B, Boegel S, Albrecht C, Bukur T, Bukur V, Holtsträter C, Ritzel C, Manninen K, Tadmor AD, Vormehr M, et al. Multi-omics characterization of the 4T1 murine mammary gland tumor model. *Front Oncol.* 2020;10:1195. doi:10.3389/fonc.2020.01195.
22. Fu X, Yang Y, Xie J, Pan X, Yang X, Du Z, Hao E. Subcutaneous inoculation position affects the immune environment in CT26 carcinomas. *Biochem Biophys Res Commun.* 2019;512(2):244–249. doi:10.1016/j.bbrc.2019.03.042.
23. Liu Y, Yang H, Li T, Zhang N. Immunotherapy in liver cancer: overcoming the tolerogenic liver microenvironment. *Front Immunol.* 2024;15:1460282. doi:10.3389/fimmu.2024.1460282.
24. Buechler MB, Teal TH, Elkon KB, Hamerman JA. Cutting edge: type I IFN drives emergency myelopoiesis and peripheral myeloid expansion during chronic TLR7 signaling. *J Immunol.* 2013;190(3):886–891. doi:10.4049/jimmunol.1202739.
25. Nguyen TH, Abidin BM, Heinonen KM. Frizzled-6 promotes hematopoietic stem/progenitor cell mobilization and survival during lps-induced emergency myelopoiesis. *STEM Cell Rep.* 2022;17(10):2303–2317. doi:10.1016/j.stemcr.2022.08.004.
26. Lefrançais E, Ortiz-Muñoz G, Caudrillier A, Mallavia B, Liu F, Sayah DM, Thornton EE, Headley MB, David T, Coughlin SR, et al. The lung is a site of platelet biogenesis and a reservoir for haematopoietic progenitors. *Nature.* 2017;544(7648):105–109. doi:10.1038/nature21706.
27. Siegel RL, Miller KD, Wagle NS, Jemal A. Cancer statistics, 2023. *CA Cancer J Clin.* 2023;73(1):17–48. doi:10.3322/caac.21763.
28. Rodell CB, Arlauckas SP, Cuccarese MF, Garris CS, Li R, Ahmed MS, Kohler RH, Pittet MJ, Weissleder R. TLR7/8-agonist-loaded nanoparticles promote the polarization of tumour-associated macrophages to enhance cancer immunotherapy. *Nat Biomed Eng.* 2018;2(8):578–588. doi:10.1038/s41551-018-0236-8.
29. Li H, Somiya M, Kuroda S. Enhancing antibody-dependent cellular phagocytosis by Re-education of tumor-associated macrophages with resiquimod-encapsulated liposomes. *Biomaterials.* 2021;268:120601. doi:10.1016/j.biomaterials.2020.120601.
30. Li Y, Cao F, Li M, Li P, Yu Y, Xiang L, Xu T, Lei J, Tai YY, Zhu J, et al. Hydroxychloroquine induced lung cancer suppression by enhancing chemo-sensitization and promoting the transition of M2-TAMs to M1-like macrophages. *J Exp Clin Cancer Res.* 2018;37(1):259. doi:10.1186/s13046-018-0938-5.
31. Rašková M, Lacina L, Kejík Z, Venhauerová A, Skaličková M, Kolář M, Jakubek M, Rosel D, Smetana K, Brábek J. The role of IL-6 in cancer cell invasiveness and metastasis—overview and therapeutic opportunities. *Cells.* 2022;11(22):3698. doi:10.3390/cells11223698.
32. Jackson WD, Giacomassi C, Ward S, Owen A, Luis TC, Spear S, Woollard KJ, Johansson C, Strid J, Botto M, et al. TLR7 activation at epithelial barriers promotes emergency myelopoiesis and lung antiviral immunity. *eLife. eLife.* 2023;12:e85647. doi:10.7554/eLife.85647.
33. Yu YR, O’Koren EG, Hotten DF, Kan MJ, Kopin D, Nelson ER, Que L, Gunn MD. A protocol for the comprehensive flow cytometric analysis of immune cells in normal and inflamed murine non-lymphoid tissues. *PLOS ONE.* 2016;11(3):e0150606. doi:10.1371/journal.pone.0150606.
34. Liu Z, Gu Y, Shin A, Zhang S, Ginhoux F. Analysis of myeloid cells in mouse tissues with flow cytometry. *Star Protoc.* 2020;1(1):100029. doi:10.1016/j.xpro.2020.100029.